







Genetic analysis of chlorophyll synthesis and degradation regulated by BALANCE of CHLOROPHYLL METABOLISM

Hiroshi Yamatani,^{1,†} Takeshi Ito ,¹ Kenji Nishimura,^{2,*} Tetsuya Yamada ,³ Wataru Sakamoto ² and Makoto Kusaba ^{1,*,\$}

¹ Graduate School of Integrated Sciences for Life, Hiroshima University, Hiroshima 739-8526, Japan

² Institute of Plant Science and Resources, Okayama University, Kurashiki 710-0046, Japan

³ Graduate School of Agriculture, Hokkaido University, Sapporo 060-8589, Japan

*Author for correspondence: akusaba@hiroshima-u.ac.jp

[†]Senior author

[‡]Present address: Institute of Crop Science, NARO, Tsukuba 305-8518, Japan.

[§]Present address: Department of Bioscience, School of Science and Technology, Kansei Gakuin University, Sanda 669-1337, Japan.

These authors contributed equally (H.Y. and T.I.)

M.K. and H.Y. conceived the original research plans. T.Y., W.S., and K.N. supervised the experiments. H.Y. and T.I. designed and performed the experiments. H.Y., T.I., and M.K. wrote the manuscript.

The author responsible for distribution of materials integral to the findings presented in this article in accordance with the policy described in the Instructions for Authors (<https://academic.oup.com/plphys/pages/general-instructions>) is: Makoto Kusaba (akusaba@hiroshima-u.ac.jp).

Abstract

Chlorophyll (Chl) serves a number of essential functions, capturing and converting light energy as a component of photosystem supercomplexes. Chl degradation during leaf senescence is also required for adequate degeneration of chloroplasts and salvaging of nutrients from senescent leaves. In this study, we performed genetic analysis to determine the functions of BALANCE of CHLOROPHYLL METABOLISM1 (BCM1) and BCM2, which control Chl levels by regulating synthesis and degradation, and STAY-GREEN (SGR)1 (also known as NON-YELLOWING1 [NYE1]) and SGR2, which encode Mg-dechelatase and catalyze Chl *a* degradation in Arabidopsis (*Arabidopsis thaliana*). Analysis of *bcm1 bcm2* revealed that both BCM1 and BCM2 are involved in the regulation of Chl levels in presenescent leaves and Chl degradation in senescing leaves. Analysis of *bcm1 bcm2 nye1 nye2* suggested that BCMs repress Chl-degrading activity in both presenescent and senescing leaves by regulating SGR activity. Furthermore, transactivation analysis and chromatin immunoprecipitation (ChIP) assay revealed that GOLDEN2-LIKE1 (GLK1), a central transcription factor regulating the expression of genes encoding photosystem-related proteins, such as light-harvesting Chl *a/b*-binding proteins (LHCPs), directly regulates the transcription of *BCM1*. LHCPs are stabilized by Chl binding, suggesting that GLKs control the amount of LHCP through transcriptional and post-translational regulation via BCM-mediated Chl-level regulation. Meanwhile, we generated a mutant of the *BCM* ortholog in lettuce (*Lactuca sativa*) by genome editing and found that it showed an early yellowing phenotype, but only a slight reduction in Chl in presenescent leaves. Thus, this study revealed a conserved but slightly diversified regulation of Chl and LHCP levels via the GLK-BCM pathway in eudicots.

Introduction

Chlorophyll (Chl) is an essential substance that captures and converts light energy and performs several functions in Chl-protein complexes (Gao et al., 2018). The major Chl, Chl a , is involved in both the capture and conversion of light energy in the core complexes of photosystems I (PSI) and II (PSII), whereas Chl b , the minor Chl, contributes to light energy capture only in the peripheral light-harvesting complexes of PSI (LHCI) and PSII (LHCII).

Chl synthesis is initiated by the conversion of glutamate to 5-aminolevulinic acid (ALA), which is catalyzed by glutamyl-tRNA synthetase, glutamyl-tRNA reductase, and glutamate 1-semialdehyde aminotransferase (Tanaka et al., 2011). ALA is then metabolized to protoporphyrin IX (Proto IX). Ferrochelatase then inserts Fe $^{2+}$ into Proto IX in the heme-synthesizing branch, whereas Mg-chelatase inserts Mg $^{2+}$ into Proto IX in the Chl-synthesizing branch, generating Mg-Proto IX. Mg-chelatase is composed of CHLH (GENOMES UNCOUPLED5; GUN5), CHLI, and CHLD subunits, the activity of which is regulated by the porphyrin-binding protein GUN4. Mg-Proto IX is subsequently metabolized to Chl a , from which Chl b is synthesized by chlorophyllide a oxygenase (CAO).

The first step in Chl a degradation involves the removal of Mg $^{2+}$ from Chl a by Mg-dechelatease STAY-GREEN (SGR) (Park et al., 2007; Ren et al., 2007; Shimoda et al., 2016). Phytol residues are removed from the resultant pheophytin by PHEOPHYTINASE (Morita et al., 2009; Schelbert et al., 2009), resulting in the formation of pheophorbide a , which is then metabolized into transparent substances, nonfluorescent chlorophyll catabolites (NCCs), or dioxobilin-type NCCs (DNCCs). Chl b is converted into Chl a via the Chl b reductases NON-YELLOW COLORING1 (NYC1) and NYC1-LIKE (NOL) (Kusaba et al., 2007; Horie et al., 2009; Sato et al., 2009), and HYDROXYMETHYL CHL a REDUCTASE (Meguro et al., 2011) then degraded in the Chl a -breakdown pathway. Mutants of Chl-degrading enzyme genes retain their green color owing to impaired Chl breakdown, although their leaves gradually die during senescence. These mutants are known as non-functional stay-green mutants and are distinguishable from delayed senescence (functional stay-green) mutants (Kusaba et al., 2013).

The amount of light-harvesting Chl a/b -binding proteins (LHCPs) (LHCI and LHCII) is controlled at both the transcriptional and posttranslational levels (Kusaba et al., 2007; Waters and Langdale, 2009; Wang and Grimm, 2015; Jia et al., 2016), with GARP (Golden2, ARR-B, Psr1) nuclear transcription factors GOLDEN2-LIKE (GLK) 1 and GLK2 acting as central transcriptional regulators of LHCP gene expression (Waters et al., 2009). LHCPs are stable only if they bind Chl into a tight fold, suggesting that LHCP content is regulated by Chl content (Paulsen et al., 1993). For example, while SGR overexpression and SGR-inducible plants show enhanced and inducible degradation of Chl and LHCP (Park et al., 2007; Wu et al., 2016; Ono et al., 2019), LHCP degradation is strongly repressed during leaf senescence in mutants

of Chl-degrading enzymes (Kusaba et al., 2007; Park et al., 2007; Sato et al., 2007; Morita et al., 2009; Sato et al., 2009; Schelbert et al., 2009).

In general, Chl levels are regulated by enzymes involved in Chl synthesis and breakdown (Tanaka et al., 2011). In addition, proteins involved in the stability of Chl-binding proteins, mutants of which show a pale-green phenotype, have also been shown to play a role in regulating Chl (Kusaba et al., 2013; Wang and Grimm, 2015). Recently, a novel post-translational regulator of Chl levels has also been reported, namely, BALANCE of CHLOROPHYLL METABOLISM (Wang et al., 2020), which is similar to CaaX proteases. Ras converting enzyme1 (RCE1)- and Sterile24 (Ste24)-class CaaX proteases are localized in the endoplasmic reticulum, where they play a role in the plasma membrane localization of proteins with a CaaX motif and translocon quality control, respectively (Majsec et al., 2017). BCMs are localized in the thylakoid membrane in chloroplasts, where they play a role in Chl synthesis and degradation (Wang et al., 2020; Zhang et al., 2020).

In *Arabidopsis* (*Arabidopsis thaliana*), there are two BCMs, BCM1 and BCM2, which have similar biochemical properties (Wang et al., 2020). BCM1 and BCM2 interact with GENOME UNCOUPLED4 (GUN4) to promote Mg-chelatase activity and Chl synthesis. They also interact with SGR to destabilize the SGR protein and repress Chl degradation. Zhang et al. (2020) suggested that CBD1 (also known as BCM1) serves as a Mg-transport protein. Although *bcm1 bcm2* double mutants were described by Wang et al. (2020) and Zhang et al. (2020), detailed genetic analyses using null alleles have not been performed so far. Therefore, precise functional differences between BCM1 and BCM2 remain unrevealed. Furthermore, genetic interactions between BCMs and SGRs have not been investigated.

In this study, we analyzed the genetic interactions between BCM1 and BCM2 and between BCMs and SGRs using double and quadruple mutants. These analyses revealed the precise functions of BCM1 and BCM2 and provided evidence for the very strict regulation of SGR activity in presenescent leaves. Furthermore, we revealed that the expression of BCM1 is directly regulated by GLK1/2 transcription factors, suggesting that GLK1/2 transcription factors regulate the amount of LHCP by upregulating the transcription of LHCP genes and stabilizing LHCP by retaining Chl levels through upregulation of BCM1 transcription. In addition, we found that this scheme is conserved in *Lactuca sativa* L. (lettuce), although the function of the BCM ortholog may differ slightly from that of BCM1 in *Arabidopsis*.

Results

BCM1- and BCM2-mediated regulation of Chl content in presenescent leaves

Plastid CaaX protease-like proteins constitute a plant-specific family (Majsec et al., 2017), of which only a few have been characterized in detail. In soybean, the CaaX protease-like protein gene G regulates seed coat coloring

and plays an important role in soybean (*Glycine max*) domestication (Wang et al., 2018). Meanwhile, Arabidopsis contains two co-orthologs, *G*, *BCM1*, and *BCM2*, which show high similarity (82% amino acid identity) with each other and retain chloroplast transit peptides and six transmembrane domains, although *BCM2* has a longer stretch at its N-terminal, suggesting that they are chloroplast membrane proteins (Wang et al., 2020; Supplemental Figure S1A). To determine the subcellular localization of *BCM1* in detail, we produced transgenic plants expressing the *BCM1* protein with a 4× MYC-tag. Isolated chloroplasts from the transgenic plants were then fractionated into thylakoid membrane and stroma + envelope fractions using density gradient centrifugation (Supplemental Figure S1B). SDS-PAGE and western blot analysis revealed signals for *BCM1* in the thylakoid membrane fraction, similar to those of other thylakoid membrane proteins, such as YELLOW VARIEGATED2 (*VAR2*; Chen et al., 2000; Takechi et al., 2000) and LHCII. This result confirms previous studies suggesting that *BCM1* is localized in the thylakoid membrane (Wang et al., 2020; Zhang et al., 2020).

Wang et al. (2020) reported that both *BCM1* and *BCM2* are involved in Chl synthesis through the regulation of Mg-chelatase activity. To genetically determine the function of *BCM1* and *BCM2* in Chl synthesis, we generated a *bcm2* mutant via genome editing using the CRISPR-Cas9 system, as only *bcm2* mutants with T-DNA insertions in the 5' upstream or untranslated regions were available (*bcm2-1* and *bcm2-2*; Figure 1A). For genome editing of *BCM2*, we designed gRNAs at the second and fourth exons and isolated *bcm2-3*, *bcm2-4*, and *bcm2-5*, which contained a 1-bp deletion in the second exon, a 9-bp deletion in the second exon, and a 1-bp insertion in the fifth exon, respectively (Figure 1A and Supplemental Figures S1A and S2A). Mutations in *bcm2-3* and *bcm2-5* cause frameshifts, suggesting that they are null mutants. Moreover, while the null mutant *bcm1-3* presented a weak pale green/low Chl content phenotype, no changes in leaf color/Chl content were observed in *bcm2-3* (Figure 1, B and C). Meanwhile, *bcm1-3 bcm2-3* showed a strong pale green/low Chl content and a retarded growth phenotype (Figure 1, B and C). Similarly, *bcm1-3 bcm2-4* and *bcm1-3 bcm2-5* showed a strong pale green/low Chl content and retarded growth, confirming the redundant functions of *BCM1* and *BCM2* in regulating Chl content, although *BCM2* contributed less than *BCM1* (Supplemental Figure S2B). This result was consistent with that reported by Zhang et al. (2020). However, Wang et al. (2020) did not observe an enhanced reduction in the Chl content in *bcm1-3 bcm2-2*. This is likely because *bcm2-2*, which has a T-DNA insertion at the 5' upstream region of *BCM2*, is a weak allele of *bcm2*. The low Chl phenotypes of *bcm1-3 bcm2-3* were also complemented by *BCM1* promoter-driven *BCM1-4*× MYC and *BCM2-4*× MYC constructs, suggesting that *BCM1* and *BCM2* have the same protein function (Supplemental Figure S3, A and B), which is further supported by lines of biochemical evidence (Wang

et al., 2020). Interestingly, *bcm1-3* and *bcm1-3 bcm2-3* had a higher Chl*a/b* ratio than Col-0, as observed by Zhang et al. (2020), suggesting that the reduction in Chl*b* was more severe than that of Chl*a* in both mutants (Figure 1C).

Wang et al. (2020) reported a slight reduction of Lhca1 and Lhcb1 in presenescent leaves of the *bcm1-3* single mutant. We extensively examined chloroplast proteins in *bcm1 bcm2* double mutants (Supplemental Figure S4). Accordingly, *bcm1-3* and *bcm2-3* showed a reduction in the protein content of PSI and PSII subunits in presenescent leaves. Moreover, this reduction was particularly prominent in LHCI and LHCII. The LHC1 level was 61%, 65%, 54%, and 72% of wild-type levels in Lhca1, Lhca2, Lhca3, and Lhca4, respectively, and the LHCII level was 46%, 33%, and 54% of wild-type levels in Lhcb1, Lhcb3, and Lhcb4, respectively. Lhca and Lhcb are the only Chl*b*-containing proteins in plant cells, which may explain the higher Chl*a/b* ratio in *bcm1* and *bcm1 bcm2* mutants (Figure 1C). PSI core complex subunits were also reduced in *bcm1 bcm2* mutants, although the PSII core complex subunits were largely unchanged. Previous studies reported that the degradation of PSII core complex subunits is regulated by THYLAKOID FORMATION1/NYC4 rather than by Chl degradation (Yamatani et al., 2013; Chen et al., 2021). It is, therefore, possible that the reduced Chl content in the *bcm1 bcm2* mutant did not affect the protein levels of the core PSII subunits. In contrast, the levels of chloroplast proteins localized in the envelope, such as TRANSLOCON AT THE INNER ENVELOPE MEMBRANE OF CHLOROPLASTS 40 (TIC40) and TIC110, showed a slight increase, whereas those in the stroma, such as HIGH-CHLOROPHYLL-FLUORESCENCE 101 (HCF101) and Rubisco large subunit, were unchanged in the *bcm1 bcm2* double mutants. Meanwhile, mRNA levels of LHCI and LHCII genes *Lhca1* and *Lhcb1.1*, and the PSI core subunit gene *PsaF*, showed no prominent reduction in presenescent leaves of *bcm1-3 bcm2-3* (Supplemental Figure S5). Overall, these findings suggest that the reduction in LHCPs and *PsaF* in the presenescent leaves of *bcm1-3 bcm2-3* was mainly caused by a posttranslational mechanism.

BCM1- and BCM2-mediated regulation of Chl degradation during leaf senescence

Previous studies have shown that BCMs are also involved in leaf yellowing (Wang et al., 2020). Therefore, we verified the functions of *BCM1* and *BCM2* during leaf senescence using null single and double mutants (Supplemental Figure S6A). While the Chl content of *bcm1-3* and *bcm2-3* decreased in a similar manner to Col-0 during dark incubation, an apparent early yellowing phenotype was observed during leaf senescence in *bcm1-3 bcm2-3*, in addition to the lower Chl content phenotype in presenescent leaves (Supplemental Figure S6, B and C). These observations suggest that single mutants of *bcm1* and *bcm2* do not exhibit an early yellowing phenotype, with *BCM1* and *BCM2* redundantly repressing leaf yellowing. Although presenescent leaves of the *BCM1* overexpressing plants (*BCM1-OE*) did not have a higher Chl

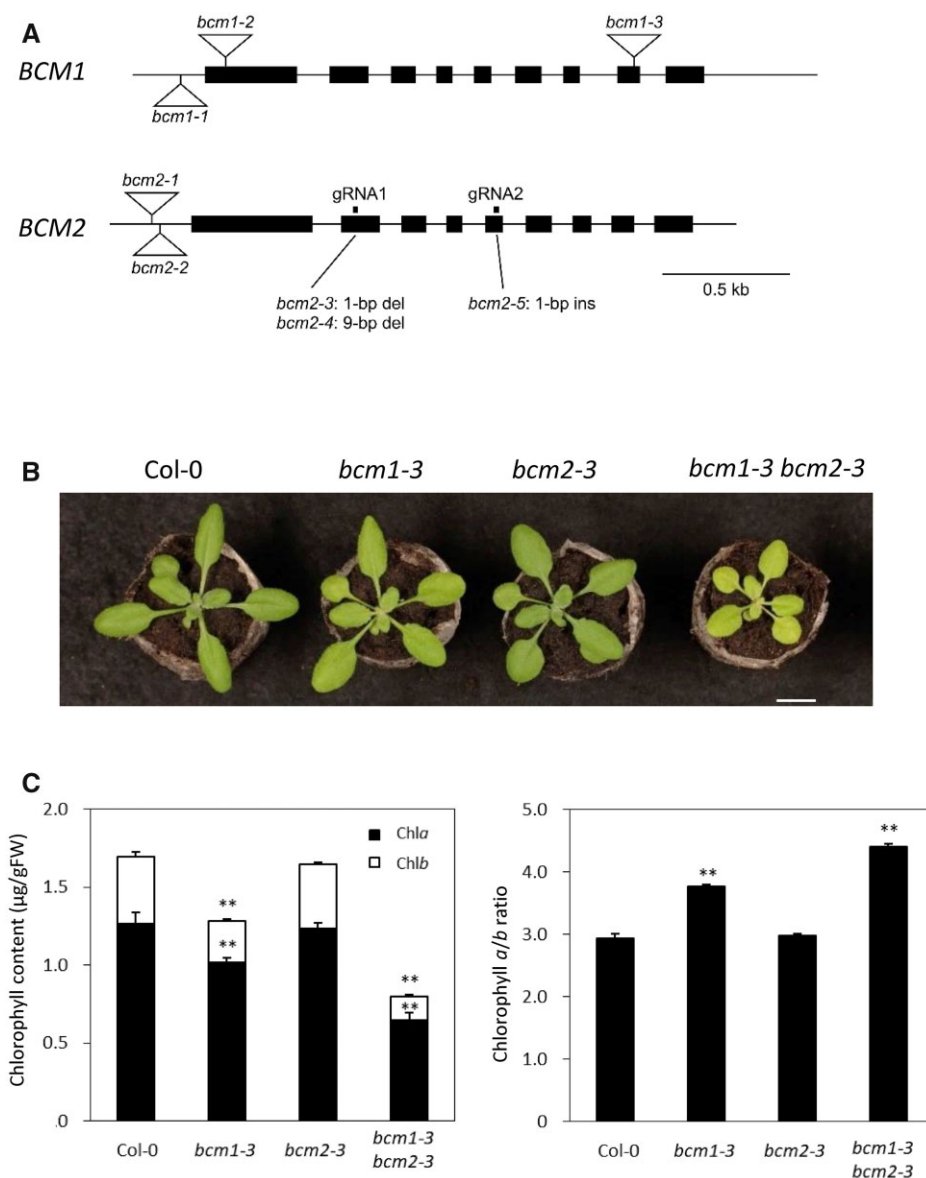


Figure 1 Characterization of the alleles of *bcm1* and *bcm2*. **A**, Structures of the *bcm1* and *bcm2* alleles. *bcm2-3*, *bcm2-4*, and *bcm2-5* were generated using the CRISPR-Cas9 system. *bcm2-3* and *bcm2-4* were obtained using gRNA1 in the second exon, while *bcm2-5* was obtained using gRNA2 in the fifth exon. Triangles indicate the T-DNA insertions. **B**, *bcm1-2*, *bcm2-3*, and *bcm1-2 bcm2-3* plants were grown for 20 days under long-day conditions at 22°C. Scale bar: 1 cm. **C**, Chl contents and the Chl *a/b* ratio of presenescent leaves of *bcm1-2*, *bcm2-3*, and *bcm1-2 bcm2-3*. Eighth leaves from the top of 27-day-old plants grown under short-day conditions were used. Error bars indicate the standard error ($n = 4$). ** $P < 0.01$ (Student's *t* test).

content than Col-0, a high Chl content was retained during dark incubation (Supplemental Figure S6, A and B). There was no statistical difference in the decrease in F_v/F_m values, reflecting PSII activity between BCM1-OE and Col-0 during dark incubation, suggesting that BCM1 represses Chl degradation, but not leaf senescence (Supplemental Figure S6D). Thus, BCM1-OE plants represent a nonfunctional stay-green line, in which Chl degradation is primarily repressed during leaf senescence, which is consistent with the observations of Wang et al. (2020). Meanwhile, in *bcm1-3 bcm2-3*, F_v/F_m values decreased much earlier than in Col-0 during dark incubation, which is congruent with its early yellowing phenotype

(Supplemental Figure S6D). Consistent with this, induction of senescence-associated genes (SAGs), such as *SGR1*, *ORESARA1* (*ORE1*), *AtNAP*, and *NYC1*, occurred sooner in *bcm1-3 bcm2-3* than in the wild-type during dark incubation (Supplemental Figure S7A). These findings suggest that leaf senescence was synchronous with Chl degradation in *bcm1-3 bcm2-3*, in contrast to BCM1-OE plants. Ono et al. (2019) previously reported that dexamethasone-induced *SGR* expression induces leaf senescence (i.e. increased expression of *ORE1* and SAGs). Although BCMs primarily act in the degradation of Chl, accelerated Chl degradation may also have induced leaf senescence in *bcm1-3 bcm2-3*.

Genetic interactions between BCM and SGR

Wang et al. (2020) previously revealed that BCM represses Chl degradation through SGR destabilization during leaf senescence. To investigate the genetic interactions between BCM and SGR, we generated a *bcm1-3 bcm2-3 nye1-1 nye2-1* mutant (*nye1-1* and *nye2-1* represent *SGR1* and *SGR2* mutants, respectively [Wu et al., 2016; Figure 2A]). Unexpectedly, the Chl content of the quadruple mutant plants was significantly higher than that of *bcm1-3 bcm2-3*, although *nye1-1 nye2-1* had a similar Chl content to that of Col-0 (Figure 2, A and C). This observation suggests that the reduced Chl content in *bcm1-3 bcm2-3* was partly caused by the degradation of Chl via SGR, although the expression of SGR was very low in presenescent leaves. In addition, *nye1-1 nye2-1* partially reversed the retarded growth of *bcm1-3 bcm2-3*, suggesting that the increased Chl content resulting from SGR impairment contributed to the restoration of photosynthesis/biomass to some extent (Figure 2A).

Next, we examined the degradation of Chl during dark incubation in *bcm1-3 bcm2-3 nye1-1 nye2-1* (Figure 2, B–D). Accordingly, the relative SPAD value of *nye1-1 nye2-1* decreased to ~75% that of the presenescent leaves 6 days after the beginning of dark treatment, while that of *bcm1-3 bcm2-3 nye1-1 nye2-1* decreased to ~40%, which was substantially lower than that of *nye1-1 nye2-1*. While BCMs are reportedly involved in the destabilization of SGR protein (Wang et al., 2020), this result suggests that BCMs repress Chl degradation through SGR-dependent and SGR-independent pathways.

Transcriptional regulation of BCM1 by GLK

As mentioned above, it has been previously suggested that BCM1 and BCM2 act as regulators of Chl content. Therefore, we analyzed light- and senescence-induced expression of BCM1 and BCM2. As a result, the expression of BCM1 was drastically reduced within 6 h of dark treatment, similar to that of *Lhcb1.1* and CAO (Supplemental Figure S7B), both of which are direct targets of GLK transcription factors (Waters et al., 2009). Expression of GLK1 and GLK2 was also drastically reduced within 6 h of dark treatment (Supplemental Figure S7B). Meanwhile, expression of BCM2 also decreased to 57.2% within 6 h of dark treatment, although an increase was observed from 4 days (Supplemental Figure S7B). Overall, the expression of BCM2 increased during extended dark incubation, suggesting that expression of BCM2 is regulated by not only light but also senescence.

To determine the transcriptional regulation of BCM1 and BCM2 by GLKs, we analyzed the expression of BCM1 and BCM2 in the *glk1 glk2*. Accordingly, the expression was reduced to 14.1% that of the wild-type, suggesting an important contribution of GLK1 and GLK2 to the expression of BCM1 in presenescent leaves (Figure 3A). Meanwhile, the expression of BCM2 was reduced to only 61.1% that of the wild-type, suggesting less of contribution to BCM2 expression (Figure 3A). These findings were also consistent with the difference in expression between BCM1 and BCM2 in response to dark treatment (Supplemental Figure S7B).

To investigate the transcriptional regulation of BCM1 by GLK1, transactivation analysis using luciferase as a reporter gene was performed, along with a chromatin immunoprecipitation (ChIP) assay (Figure 3, B and C). When the BCM1 promoter-LUC construct was transiently introduced into mesophyll protoplasts together with the GLK1-4× MYC construct, luciferase activity was elevated 13.0-fold compared to the noneffector controls. The luciferase activities of *Lhca1*, *Lhcb1.1*, *Lhcb2.2*, and CAO, which are reported to be directly regulated by GLK1, were also notably elevated by 105.6-, 6.6-, 113.3-, and 9.3-fold, respectively, following the introduction of the GLK1-4× MYC construct (Figure 3B; Waters et al., 2009). A ChIP assay was subsequently performed using GLK1-4× MYC overexpressing plants. Accordingly, GLK1-binding was observed with promoters of known GLK1-target genes, *Lhca1*, *Lhcb1.1*, *Lhcb2.2*, and CAO, but not with the promoter of the non-GLK1 target gene ACTIN8, confirming the observation by Waters et al. (2009). The BCM1 promoter did not contain a perfect GLK1-binding consensus sequence (CCAATC), but instead contained five 1-bp-substituted sequences (Figure 3C). Therefore, we analyzed four fragments of the promoter region (designated A–D) and one fragment of the structural gene region (E) for GLK1 binding. All four fragments in the promoter region, but not in the structural gene region, were enriched for GLK1 binding (Figure 3C), suggesting that GLK1 selectively binds to the promoter region of BCM1. A similar result was obtained in an independent experiment (Supplemental Figure S8). These observations suggested that BCM1 is a direct target of GLK1, consistent with a previous study that identified BCM1 as an early GLK1-inducible gene (Waters et al., 2009). We also performed a ChIP analysis of the BCM2 promoter for GLK1 binding. The BCM2 promoter harbored possible GLK1-binding motifs, but no statistically significant enrichment was observed in any of the promoter fragments examined (Supplemental Figure S9).

Analysis of the BCM ortholog in lettuce

To determine whether the function of BCM is conserved in other species, we analyzed lettuce mutants of BCM and SGR. Lettuce contains only single genes for BCM (*LsBCM*), SGR (*LsSGR*), and GLK (*LsGLK*) in its genome (Supplemental Figures S10, A–C and S11). Therefore, we generated *LsBCM* and *LsSGR* mutants via CRISPR-Cas9, using two guide RNAs (Figure 4A). The resulting *lsbcm-1* and *lsbcm-2* mutants contained 1-bp insertions at the 411th and 216th nucleotides from the initiation codon, respectively. These insertions caused frameshifts, suggesting that they were null mutants. *lssgr-1* and *lssgr-2* contained a 1-bp insertion and 12-bp deletion at the 39th and 199–210th nucleotides from the initiation codon, respectively. *lssgr-1* was also considered a null mutant due to frameshifts (Figure 4A).

Both *lssgr-1* and *lssgr-2* showed a strong stay-green phenotype similar to the *nye1-1 nye2-1* double mutant in Arabidopsis during both dark-induced and natural senescence, confirming that *LsSGR* is a single-copy gene with the same function in lettuce (Figure 4, B and C and

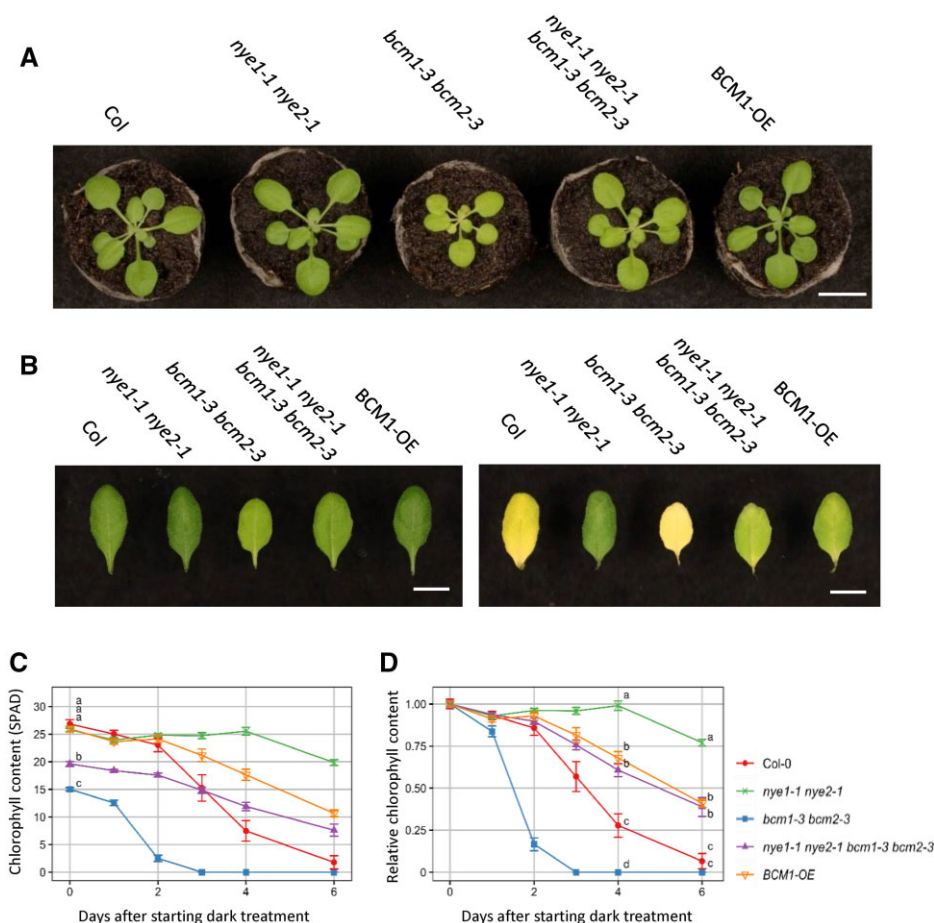


Figure 2 Leaf color and senescence phenotypes of the *bcm nye* quadruple mutant. A, Twenty-two-day-old plants were grown at 22°C under short-day conditions. B, Leaves before and 6 days after dark incubation. Seventh leaves from the top of 28-day-old plants grown at 22°C under short-day conditions were detached and incubated at 22°C in the dark. C and D, Changes in Chl content with time during dark incubation. Data indicate SPAD values and relative values to presenescent leaves. Scale bar: 1 cm.

Supplemental Figure S12, A and B). Meanwhile, *lsbcm-1* and *lsbcm-2* also showed an early yellowing phenotype during dark-induced and natural senescence, similar to *bcm1-3 bcm2-3* in Arabidopsis. Furthermore, the *lsbcm-1 lssgr-1* and *lsbcm-2 lssgr-2* double mutants showed a stay-green phenotype similar to that of the *bcm1-3 bcm2-3 nye1-1 nye2-1* quadruple mutant in Arabidopsis. These observations suggest that the function of BCM in Chl degradation during leaf senescence is conserved between lettuce and Arabidopsis plants. However, the early yellowing phenotype of *lsbcm-1* was strongly suppressed by *lssgr-1*, suggesting that LsBCM represses Chl degradation almost exclusively through downregulation of SGR function in lettuce, unlike in Arabidopsis (Figure 4, B and C and Supplemental Figure S12B).

The *bcm1-3 bcm2-3* mutant in Arabidopsis showed a prominent pale green phenotype (Figure 1B), whereas presenescent leaves of *lsbcm-1* did not (Supplemental Figure S12B). Detailed analysis using nonsenescent leaves from nine individuals further revealed a slight but significantly lower Chl content in presenescent leaves of *lsbcm-1* compared

with the wild-type ($P < 0.05$, Tukey's multiple comparison test) (Supplemental Figure S13A). These observations suggest that BCM in lettuce is involved in Chl synthesis in presenescent leaves, but its contribution is limited. In addition, there was no significant difference in Chl content between presenescent leaves of *lsbcm-1* and *lsbcm-1 lssgr-1*, suggesting that SGR does not play a role in Chl degradation in presenescent lettuce leaves (Supplemental Figure S13, A and B).

Next, we analyzed the changes in expression of LsBCM, LsGLK, LsLhca1, and LsSGR over time during dark incubation (Figure 4D). Similar to GLK1 and GLK2 in Arabidopsis, the expression of LsGLK decreased sharply in response to light depletion treatment, while downregulation of LsBCM was slightly slower than that of BCM1 in Arabidopsis. One LHCP gene, *LsLhca1*, also showed a very fast response to light depletion, whereas the induction rate of LsSGR was low (2.6-fold) during dark incubation. In contrast, the expression of SGR1 in Arabidopsis increased more than 10-fold even after 4 days of dark treatment, when leaves were yet to become fully senescent (Supplemental Figure S7A). To investigate the role of GLK in LsBCM and LsLhca1 expression,

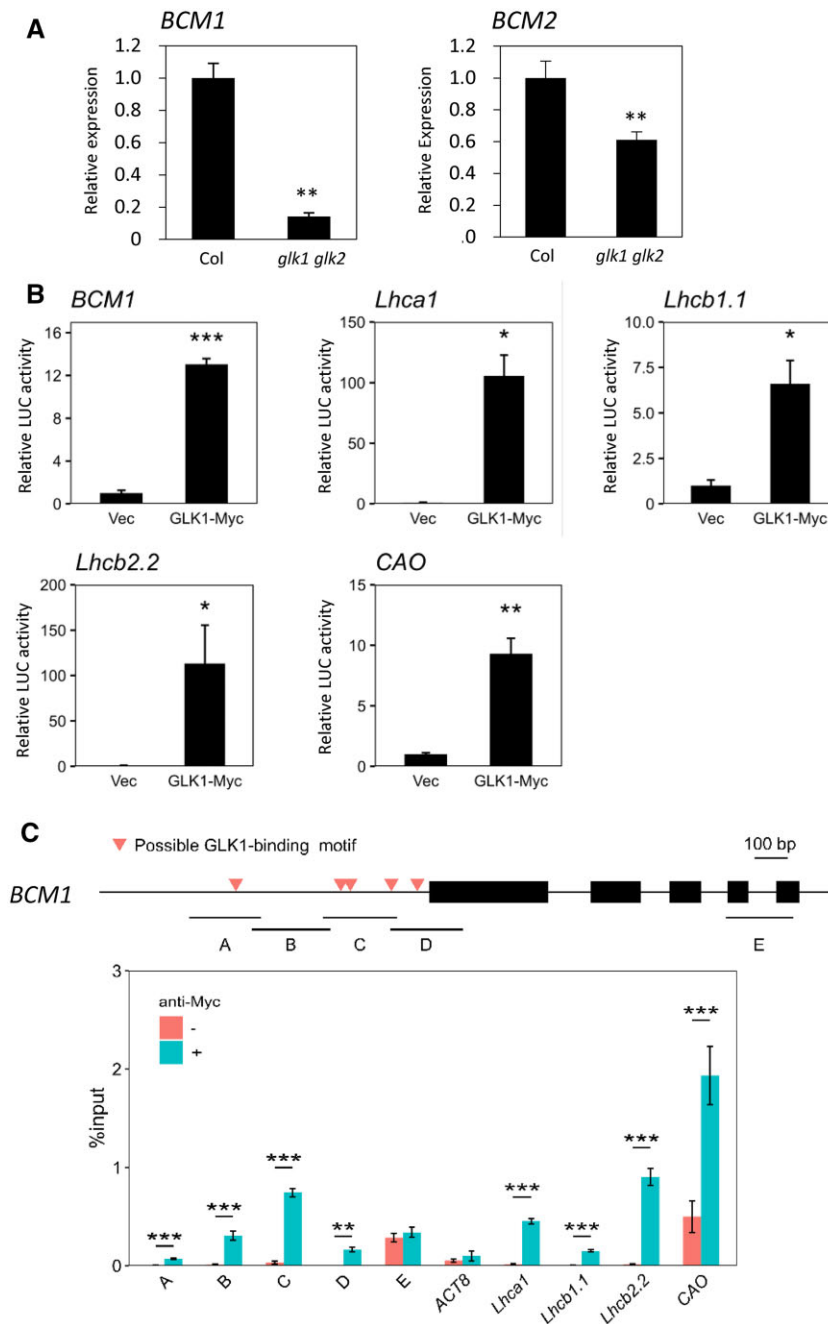


Figure 3 Direct regulation of *BCM1* expression by GLK1. A, RT-qPCR analysis of *BCM* expression in presenescent leaves of *glk1 glk2*. ** $P < 0.01$ ($n = 4$). Seventh to eighth leaves from the top of 25-day-old plants grown at 22°C under short-day conditions were used. B, Transactivation of photosynthesis-related genes by GLK1. Constructs containing luciferase genes driven by promoters of *BCM1* and known GLK1-target genes were transiently introduced into *Arabidopsis* mesophyll protoplasts together with GLK1-4 × MYC constructs (GLK1-Myc). “Vec” represents a control into which the luciferase reporter construct and an empty effector vector were introduced. C, ChIP-qPCR analysis of GLK1 binding to the *BCM1* promoter was performed using GLK1-4 × MYC overexpressing plants. The upper panel shows the gene structure of *BCM1*. Red triangles indicate the positions of possible GLK1-binding sequences. Black boxes represent exons. A–E represent DNA regions used in ChIP-qPCR analysis. The lower panel shows the results of ChIP-qPCR analysis. Fold enrichment is indicated as the % input. ** and *** $P < 0.01$ and $P < 0.001$, respectively (Student’s *t* test).

transactivation assays were performed using lettuce mesophyll protoplasts. Transient introduction of the LsGLK-4 × MYC construct significantly increased luciferase activity from the *LsBCM* and *LsLhca1* promoters, suggesting that expression of *BCM* and *Lhca1* is also directly regulated by GLK in lettuce (Figure 4E).

Discussion

In this study, we investigated the functions of *BCM1* and *BCM2* in Chl regulation using null double mutants. We found that *bcm2* null mutations prominently enhanced the pale green phenotype of *bcm1*, suggesting that both *BCM1* and *BCM2* play a role in regulating Chl levels in

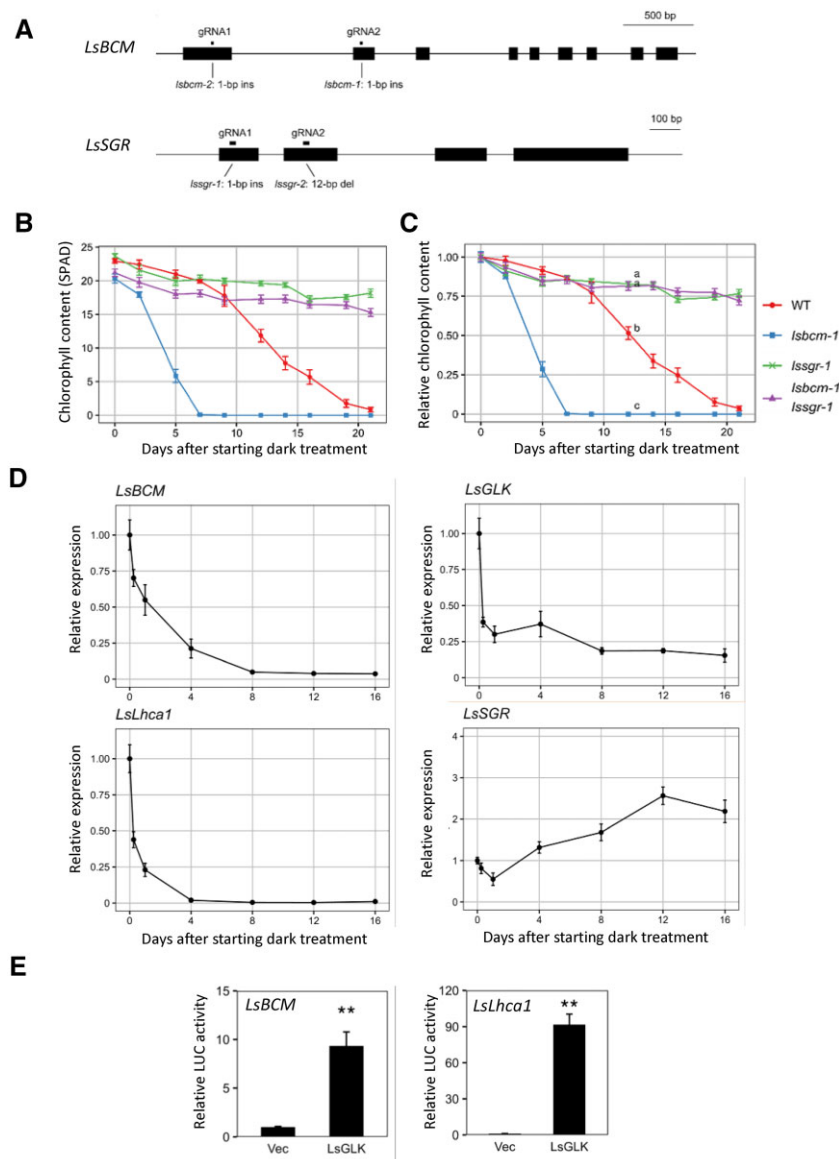


Figure 4 Functional analysis of the BCM ortholog in lettuce. A, Structures of *lsbcm-1*, *lsbcm-2*, *lssgr-1*, and *lssgr-2* mutants generated using CRISPR-Cas9-based genome editing. *lsbcm-1* and *lsbcm-2* were obtained using gRNA1 in the first exon and gRNA2 in the second exon. *lssgr-1* and *lssgr-2* were obtained using gRNA1 in the first exon and gRNA2 in the second exon. B and C, Changes in Chl content with time during dark incubation. Third leaves of three-week-old plants incubated at 22°C in the dark were used. B and C indicate SPAD values and relative values to presenescent leaves, respectively. D, Changes in gene expression of *LsBCM*, *LsGLK*, *LsLhca1*, and *LsSGR* with time. Lettuce leaves were incubated in the dark as described in panel B. E, Transactivation of *LsBCM* and *LsLhca1* expression by *LsGLK1*. Constructs carrying luciferase genes driven by promoters of *LsBCM1* and *LsLhca1* were transiently introduced into lettuce mesophyll protoplasts together with *LsGLK1* constructs. “Vec” represents a control into which the luciferase reporter construct and an empty effector vector were introduced. $n = 3$. ** $P < 0.01$ (Student’s t test).

presenescent leaves, although the single *bcm2* mutant showed no such phenotype. Wang et al. (2020) did not observe such a function of BCM2, likely because the *bcm2-2* allele that they used was a weak allele. During leaf senescence, *bcm1* and *bcm2* single mutants showed no obvious early yellowing phenotype, in contrast to their double mutants, which did so prominently, suggesting that BCM1 and BCM2 redundantly repress Chl degradation during leaf senescence, which is consistent with the conclusion of Wang et al. (2020).

Analysis of a quadruple mutant carrying mutations in *SGR1* and *SGR2* (*nye1-1 nye2-1*) as well as *bcm1-3 bcm2-3*

further revealed that loss-of-function mutations in *SGRs* suppressed the early yellowing phenotype of *bcm1 bcm2*, suggesting that *SGRs* act downstream of *BCMs*. However, retention of Chl content in the quadruple mutant was lower than that in *nye1-1 nye2-1*, suggesting that *BCMs* repress *SGR*-dependent and *SGR*-independent Chl degradation pathways.

It is well accepted that the upregulation of *SGR* during leaf senescence induces Chl degradation and subsequent LHCP degradation during dark-induced leaf senescence (Park et al., 2007; Ren et al., 2007; Sato et al., 2007; Ono et al.,

2019). Our study suggests that the reduced expression of *BCM1* is also one of the initial steps in leaf yellowing. A reduction in *BCM* expression in response to dark treatment may stabilize *SGR* proteins and facilitate Chl degradation by *SGR*. Particularly in lettuce, this regulation seemed more important because the induction rate of *SGR* expression during dark incubation was only 2.6-fold (Supplemental Figure S4D). Since the expression of *BCM2* tended to increase during the late stage of leaf senescence in *Arabidopsis*, *BCM2* is also thought to contribute to the fine-tuning of Chl degradation during late senescence.

Unexpectedly, presenescent leaves of the quadruple mutant *bcm1-3 bcm2-3 nye1-1 nye2-1* had a higher Chl content than those of *bcm1-3 bcm2-3*, implying that *SGR* contributed to the low Chl content of presenescent leaves in *bcm1-3 bcm2-3*. Although the expression of *SGR* in the presenescent leaves was very low, it is thought that a small amount of *SGR* protein resulted in the degradation of Chl in the presenescent leaves of *bcm1-3 bcm2-3*. Meanwhile, the Chl content of the presenescent leaves of *nye1 nye2* was no higher than that of Col-0, suggesting that *BCMs* eliminated *SGR* activity completely in wild-type presenescent leaves. Although it has been hypothesized that there is almost no *SGR* expression in presenescent leaves and that induction of *SGR* expression causes Chl degradation during leaf senescence, our results suggest that the Chl-degrading activity of *SGR* is strictly and securely regulated in presenescent leaves.

In this study, we revealed that *GLK1*, the central transcription factor in regulation of expression of photosynthesis-related genes, directly regulates expression of *BCM1* in *Arabidopsis*, confirming that *BCM1* is one of the important machineries regulating photosynthesis activity. Figure 5 summarizes the proposed Chl/photosynthesis regulation via the *GLK-BCM* pathway. Expression of *BCMs* is directly regulated by *GLK* transcription factors, which are known to regulate the expression of nuclear photosynthetic genes in *Arabidopsis* (Waters et al., 2009). Light activates the transcription of *BCMs* via *GLK1* and *GLK2*, resulting in Chl synthesis via the Mg-chelatase *GUN5* and its activator *GUN4* and repression of Chl degradation by destabilization of the Mg dechelatase *SGR*, securing photosynthetic performance. Furthermore, considering that the stability of LHCPs (LHCI/LHCII) is regulated by Chl content (Kusaba et al., 2013), *GLKs* are thought to regulate the amount of LHCP through transcriptional and posttranslational pathways: direct transcriptional activation of LHCP genes and stabilization of LHCP proteins via regulation of Chl synthesis/degradation by *BCMs*.

Mutants of *BCM* orthologs in soybean and tomato (*Solanum lycopersicum*) showed pale green and early yellowing phenotypes similar to *bcm1 bcm2* in *Arabidopsis*, suggesting that the function of *BCM* in Chl degradation is conserved during evolution (Liu et al., 2020, 2021). However, the *BCM*-mediated regulation of Chl levels in lettuce was somewhat different from that in *Arabidopsis*. *lsbcm* showed

an early yellowing phenotype during leaf senescence, similar to the *bcm1 bcm2* mutant in *Arabidopsis*. However, it showed only a very slight reduction in Chl content in presenescent leaves, suggesting that the contribution of *BCM* to Chl synthesis and degradation in presenescent leaves is limited in lettuce. Moreover, mutants of *BCM* orthologs in soybean and tomato showed an obvious pale green phenotype, suggesting that the functions of *BCM* are similar to those of *Arabidopsis* (Liu et al., 2020, 2021).

Arabidopsis contains several chloroplast-localized CaaX protease-like proteins other than *BCMs*. Of these, only *SNOWY COTYLEDON4 (SCO4)* has been analyzed so far, the mutant of which has albino cotyledons (Albrecht-Borth et al., 2013). Although Wang et al. (2020) reported that *BCMs* bind *GUN4* and *GUN5* to promote Mg-chelatase activity and *SGR* to destabilize the *SGR* protein, the precise biochemical function of *BCMs* has yet to be elucidated, including whether *BCMs* possess protease activity. Yeast, mammals, and plants share the CaaX proteases *RCE1* and *STE24*, whereas *BCM* does not exist in the green alga *Chlamydomonas*. Therefore, it has been suggested that *BCM* evolved in association with the acquisition of the Chl degradation function of *SGR*. However, *SGR* is involved in pheophytin synthesis rather than Chl degradation in *Chlamydomonas* (Chen et al., 2019; Wang et al., 2020). Chloroplast-localized CaaX protease-like proteins are highly divergent; therefore, their biochemical functions may also be diverse. Therefore, further studies on the function of this protein family are warranted.

Materials and methods

Plant materials and growth conditions

Arabidopsis (A. thaliana) accession Col-0 was used as the wild-type. The *bcm1-3* (SALK_058830C), *glk1 glk2* carrying *LhGR-N (4c)* inducible expression transgene (CS9907) and *GLK1* overexpression line (CS9905) were obtained from the *Arabidopsis* Biological Resource Center. *glk1 glk2* was obtained by backcrossing CS9907 with Col-0 to remove the *LhGR-N (4c)* transgene. *Arabidopsis* plants were grown on Jiffy-7 peat pellets (33 mm in diameter; Jiffy Products International AS, Norway) at 22°C under long- (16 h light/8 h dark; 16L/8D) or short-day conditions (10L/14D) with 100 $\mu\text{mol photons s}^{-1} \cdot \text{m}^{-2}$. Lettuce (*L. sativa*) cultivar Greenwave (Takii seed, Japan) was used as the wild-type lettuce. Plants were grown on Jiffy-7 peat pellets (33 or 44 mm in diameter) at 22°C under long-day conditions (16L/8D) with 170–200 $\mu\text{mol photons s}^{-1} \cdot \text{m}^{-2}$.

For dark treatment of *Arabidopsis* plants, leaves were detached and incubated in 24-well plates under high humidity in the dark at 22°C. For dark treatment of lettuce plants, leaves were detached and incubated in square petri dishes under high humidity in the dark at 26°C.

Generation of mutant and transgenic plants

bcm2-3, *bcm2-4*, and *bcm2-5* mutants were generated using the CRISPR-Cas9 system. Two guide RNA, gRNA1 and

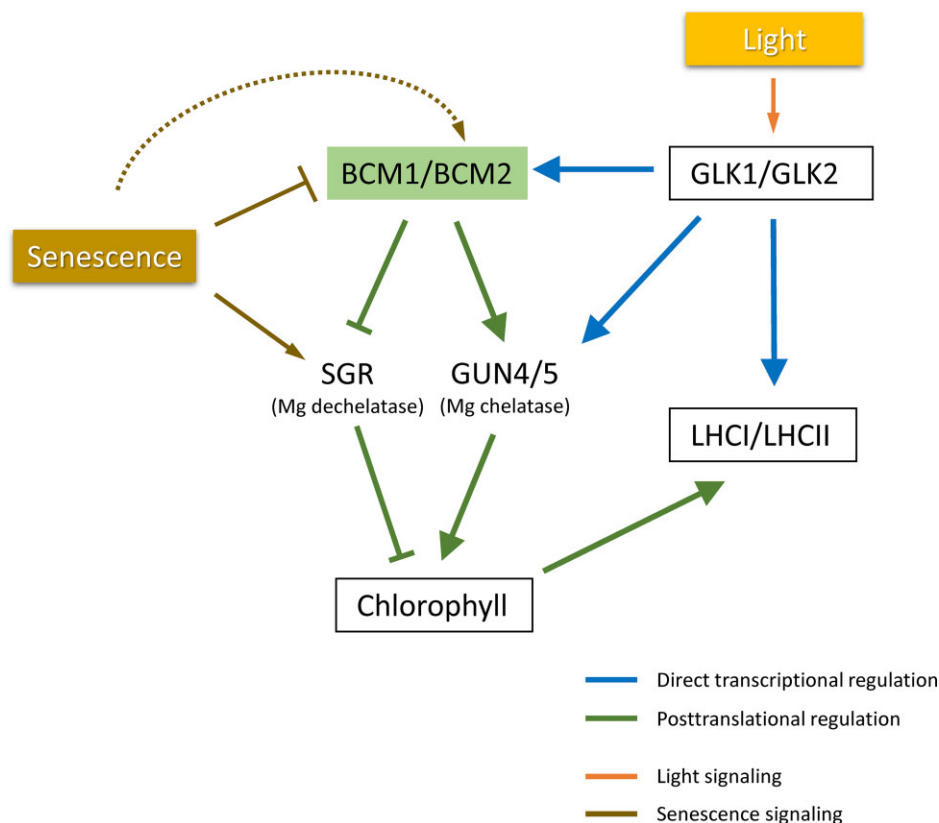


Figure 5 Schematic depiction of the GLK-BCM pathway that regulates Chl and LHCP levels in response to environmental factors in Arabidopsis. BCM is required for full activation of GUN4/5 (Chl synthesis) and destabilization of the SGR protein (repression of Chl degradation; Wang et al., 2020). GLKs control the amount of LHCP (LHCI/LHCII) via direct transcriptional regulation of (i) LHCP apoprotein genes and (ii) BCM genes, regulating levels of Chl and stabilizing LHCP. During dark-induced leaf senescence, the reduction in BCM expression caused by the rapid decrease in GLK expression in response to dark treatment is also thought to play a role in the onset of leaf yellowing. Meanwhile, expression of BCM2 is upregulated during the late stage of leaf senescence, thereby fine-tuning the Chl content.

gRNA2, were designed using the “Focas” website (Osakabe et al., 2016) and CRISPR direct (<https://crispr.dbcls.jp/>). The oligonucleotides for gRNA1 or gRNA2 were cloned into the *Bsa*I site of pEgP126_Paef1-2A-GFBS2 (Osakabe et al., 2016) and the *Aar*I site of pKI1.1R (Tsutsui and Higashiyama, 2016), respectively. Null segregants of the CRISPR-Cas9 transgene were used as *bcm2* mutants. The primers used for gRNA are shown in Supplemental Table S1.

For complementation analysis, constructs expressing *BCM1-4 × Myc* or *BCM2-4 × Myc* were generated under control of the *BCM1* promoter as follows. The multiple cloning site and NOS terminator of pMOE (Fukazawa et al., 2021) was cloned into the *Not*I and *As*I sites of pENTR (Thermo Fisher Scientific, Waltham, MA, USA), giving pENTR-MCS-NOST. The coding region of BCMs was then amplified by PCR using cDNA as a template and subcloned between the *Not*I and *Xba*I sites of pMOE *4 × Myc*, giving pMOE-*BCM1-4 × Myc* and pMOE-*BCM2-4 × Myc*, respectively. DNA fragments containing BCM and *4 × Myc* were then amplified and cloned between the *Hind*III and *Xba*I sites of pENTR-MCS-NOST, giving pENTR-*BCM1-4 × Myc* and pENTR-*BCM2-4 × Myc*, respectively. The promoter regions of *BCM1* (−979 to −1 bp; +6, translation start site) were amplified by

PCR using the genome DNA as a template then cloned between the *Not*I and *Hind*III sites of pENTR-*BCM1-4 × Myc* and pENTR-*BCM2-4 × Myc*, giving pENTR-*BCM1pro:BCM1-4 × Myc* and pENTR-*BCM1pro:BCM2-4 × Myc*, respectively. These entry constructs were then recombined into the destination binary vector pGWB601 (Nakamura et al., 2010) using Gateway LR Clonase II Enzyme mix (Thermo Fisher Scientific). To generate *BCM1* overexpression plants (*BCM1-OE*), the promoter region of *AtUBQ10* (−636 to −1 bp; +1, translation start site) was amplified by PCR and assembled into pENTR *BCM1-4 × Myc* using NEBuilder (New England Biolabs, Ipswich, MA, USA). These entry constructs were then recombined into the destination binary vector pGWB601 using Gateway LR Clonase II Enzyme mix. Arabidopsis plants were transformed based on the floral dip method using *Agrobacterium tumefaciens* strain EHA105. *lsbcm*, *lssgr*, and *lsbcm lssgr* mutants were generated using the CRISPR-Cas9 system as follows. Oligonucleotides of gRNAs designed using CRISPR direct were cloned into the *Bbs*I site of pENTR-*AtU6gRNA2* (Nobusawa et al., 2021). The gRNA expression cassette of pENTR-*AtU6gRNA2* with gRNA *LsBCM* was then digested with *Pac*I and *Pvu*I, and inserted into the *Pac*I site of pENTR-*AtU6gRNA2* with *LsSGR* gRNA in the

same direction to generate an entry vector carrying gRNA expression cassettes of both *LsBCM* and *LsSGR*. The constructs were then recombined using Gateway technology into the destination vector pGWB401_AtRPS5A-Cas9, which was constructed by subcloning a RPS5A promoter:Cas9:HSP terminator cassette from pGWB601_AtRPS5A-Cas9 into pGWB401 (Nakamura et al., 2010). Lettuce transformation was performed as described by Sun et al. (2006) with slight modifications. In this study, *A. tumefaciens* strain EHA105 and carbenicillin were used instead of GV2260 and augmentin. The primers used for gRNA are shown in Supplemental Table S1.

Measurement of senescence parameters

The foliar Chl content was measured nondestructively using a SPAD-502 Chl meter (Konica Minolta, Tokyo, Japan). For measurement of Chl a and Chl b contents, pigments were extracted from leaves using 80% (v/v) acetone after leaves were frozen and pulverized to a powder using TissueLyser II (Qiagen, Hilden, Germany). Chl a and Chl b levels were determined according to Wellburn (1994). F_v/F_m values were measured using a Junior PAM Chl fluorometer (Walz, Hilden, Germany) according to Kohzuma et al. (2017).

RNA extraction and quantitative reverse-transcriptase PCR analysis

Total RNA was extracted using TRI reagent (Molecular Research Center) according to the manufacturer's instructions. First-strand cDNA was synthesized from 100 to 500 ng total RNA using ReverTra Ace qPCR RT Master Mix (Toyobo, Osaka, Japan). Quantitative reverse-transcriptase PCR (RT-qPCR) was performed using KAPA SYBR FAST qPCR kit (Roche, Basel, Switzerland) and Rotor-Gene Q 2PLEX (Qiagen). RT-qPCR conditions were as follows: initial denaturation at 95°C for 30 s, followed by 35–50 cycles at 95°C for 5 s, ending with 60°C for 30 s. Transcript levels were normalized to those of *ACTIN8* (*ACT8*) and *LsACT7* in *Arabidopsis* and lettuce, respectively. Data analysis was performed using the Comparative CT Method (also known as the $\Delta\Delta$ CT Method). The primers used for RT-qPCR are shown in Supplemental Table S1.

Chloroplast isolation and fractionation

Intact chloroplasts were isolated according to Olinares et al. (2010) with slight modifications. Mature rosette leaves from 4-week-old *Arabidopsis* plants were briefly homogenized in grinding medium (50 mM HEPES-KOH, pH 8.0, 330 mM sorbitol, 2 mM EDTA) then filtered through two layers of miracloth (Merck Millipore, Burlington, MA, USA). The crude plastids were purified by centrifugation at $2,380 \times g$ on 30%–80% Percoll cushions (Percoll in 0.6% Ficoll, 1.8% polyethylene glycol) for 15 min then washed with five volumes of the grinding medium. After lysing in chloroplast isolation buffer (10 mM Tricine-KOH, pH 7.5, 0.6 M sucrose), the chloroplasts were disrupted by freeze–thaw treatment (Chu and Li, 2011). The sucrose concentration of the chloroplast isolation buffer was then reduced to 0.2 M, and the lysates

were fractionated into thylakoid and stroma + envelope fractions.

Protein analysis

Frozen leaf samples were pulverized into a powder using TissueLyser II (Qiagen) and suspended in four volumes of $2 \times$ SDS sample buffer (125 mM Tris–HCl, pH 6.8, 4% [w/v] SDS, 4% [v/v] β -mercaptoethanol, 1% [w/v] bromophenol blue, 20% [v/v] glycerol). Samples were then diluted 10-fold with $1 \times$ SDS sample buffer and subjected to SDS-PAGE analysis (Tris/Glyc buffer) with or without thermal denaturation, and transferred onto an Immobilon-P transfer membrane (Millipore) (Yamatani et al., 2018). Membranes were incubated with anti-Lhca1, anti-Lhcb1, anti-Lhcb3, anti-Lhcb4, anti-PsaL, anti-D2, anti-TIC40, anti-HCF101 (Agrisera), anti-Myc (MBL), anti-CP1 (Tanaka et al., 1991), anti-PsaF (provided by Y. Takahashi), anti-D1 (Kato et al., 2012), anti-VAR2 (Sakamoto et al., 2003), or anti-TIC110 antibody (Kikuchi et al., 2013), followed by horseradish peroxidase-conjugated secondary antibody. Chemiluminescence was detected using ECL Prime western blotting detection reagents (Cytiva) and quantified using Odyssey Fc imaging system and Image Studio software (LI-COR biosciences). The Rubisco large subunit was visualized using Coomassie brilliant blue G-250 staining on SDS-PAGE gel.

Transient transfection and reporter gene assay

Arabidopsis mesophyll protoplasts were isolated according to Yoo et al. (2007) with slight modifications. Lettuce mesophyll protoplasts were isolated from the third true leaf of 3-week-old plants. Protoplasts were transfected using reporter (4 μ g), effector (4 μ g), and reference plasmids (1 μ g) then incubated at 22°C for 16 h under continuous light in 12-well tissue culture plates. Firefly and Renilla luciferase activities were then measured using the dual-luciferase reporter assay system and GloMax 20/20 luminometer (Promega, Madison, WI, USA). Coding regions of *GLK1* and *LsGLK* were amplified by PCR and cloned into pMOE then used as effector plasmids. A multiple cloning site, luciferase gene, and NOS terminator of the promoter-less LUC vector were amplified by PCR then subcloned into pENTR, giving pENTR-LUC-NOST. To construct reporter plasmids, the promoter regions of *BCM1* (–979 to +6 bp relative to the translation start site), *Lhca1* (–1000 to +6 bp), *Lhcb1.1* (–1014 to +6 bp), *Lhcb2.2* (–1001 to +6 bp), *CAO* (–1045 to +6), *LsBCM* (–1811 to +6), and *LsLhca1* (–1055 to +27) were amplified by PCR then cloned into pENTR-LUC-NOST. pPTRL, which expresses Renilla LUC under control of the CaMV 35S promoter, was used as a reference plasmid.

ChIP

ChIP was performed according to Saleh et al. (2008) with slight modifications. Samples were sonicated using Microson XL 2000 (Misonix Incorporated, USA). Dynabeads Protein G (Thermo Fisher Scientific; 100 μ L/sample) was used for immunoprecipitation instead of Protein A agarose beads and pre-equilibrated with nuclei lysis buffer with 5 mg/mL BSA

instead of salmon sperm. Anti-Myc antibody (MBL, 5 μ L) was added to the 10-fold diluted samples and incubated overnight at 4°C. qPCR was performed using a KAPA SYBR FAST qPCR kit (Roche) and Rotor-Gene Q 2PLEX (Qiagen). qPCR conditions were as follows: initial denaturation at 95°C for 30 s, followed by 45–50 cycles at 95°C for 5 s, ending with 60°C for 30 s. qPCR data were normalized using the percentage of input method. The primers used for RT-qPCR are shown in [Supplemental Table S1](#).

Prediction of transit peptide and transmembrane regions

Transit peptide sequences were predicted using ChloroP version 1.1 Server (<http://www.cbs.dtu.dk/services/ChloroP/>). Transmembrane regions of BCM1 were predicted using TMHMM Server version 2.0 (<http://www.cbs.dtu.dk/services/TMHMM/>). The amino acid sequences of the BCMs were aligned ([Supplemental Figure S11](#)) then regions corresponding to the transmembrane regions of BCM1 were regarded as the transmembrane regions of BCM2.

Phylogenetic tree construction

Neighbor-joining phylogenetic trees of the BCM, SGR, and GLK proteins were constructed using MEGA X and CLUSTAL W for amino acid sequence alignment. The evolutionary distances were computed using the Poisson correction method in units of the number of amino acid substitutions per site.

Statistical analysis

Student's *t* test and Tukey's multiple comparison analysis were performed using R software (version 3.6.3 or 4.1.0).

Accession numbers

Sequence data were deposited in the Arabidopsis Genome Initiative or National Center for Biotechnology Information under the following accession numbers: ACT8 (AT1G49240), APRR2 (AT4G18020), ARR1 (AT3G16857), BCM1 (AT2G35260), BCM2 (AT4g17840), CAO (AT1g44446), GLK1 (AT2G20570), GLK2 (AT5G44190), *Lhca1* (AT3g54890), *Lhcb1.1* (AT1G29920), *Lhcb2.2* (AT2g05070), NAP (AT1G69490), NYC1 (AT4G13250), ORE1 (AT5G39610), *PsaF* (AT1G31330), RCE1 (AT2G36305), SGR1/NYE1 (AT4G22920), SGR2/NYE2 (AT4G11910), SGRL (AT1G44000), STE24 (AT4G01320), *LsACT7* (LOC111897580, LOC111909684, LOC111882438), *LsBCM* (LOC111918094), *LsCAO* (LOC111911963), *LsGLK* (LOC111886262), *LsLhca1* (LOC111877237), *LsLhcb1* (LOC111888054), *LsSGR* (LOC111920775), *LsSGRL* (LOC111901931), *LsAPRR2-like* (LOC111897177), *LsARR1-like* (LOC111914139), *GmG* (Glyma.01G198500), *GmGL* (Glyma.11G043400), *GmGLK1* (Glyma.13G294300, Glyma.12G206600, Glyma.06G289300, Glyma.12G117700), *GmSGR1* (Glyma.11G027400), *GmSGR2* (Glyma.01G214600), *S1BCM/G* (LOC101260158), *S1GLK1* (LOC101055587), *S1GLK2* (LOC101055613), *S1SGR1* (LOC778212), and *S1SGR2* (LOC101268214).

Supplemental data

The following materials are available in the online version of this article.

SupplementalFigure S1. Protein structures and subcellular localization of BCM1 and 2.

SupplementalFigure S2. Mutations and phenotypes of the *bcm* mutants.

SupplementalFigure S3. Complementation of the *bcm1 bcm2* phenotype by BCM1 and BCM2.

SupplementalFigure S4. Western blot analysis of chloroplast proteins in presenescent leaves of *bcm1 bcm2*.

SupplementalFigure S5. Expression of photosynthesis-related genes in presenescent leaves of *bcm1 bcm2*.

SupplementalFigure S6. Chlorophyll degradation in *bcm* mutants and BCM1 overexpressing plants during leaf senescence.

SupplementalFigure S7. Expression of senescence- and photosynthesis-related genes during dark incubation.

SupplementalFigure S8. ChIP-qPCR analysis of GLK1 binding to the BCM1 promoter.

SupplementalFigure S9. ChIP-qPCR analysis of GLK1 binding to the BCM2 promoter.

SupplementalFigure S10. Neighbor-joining trees of BCM, SGR, and GLK families.

SupplementalFigure S11. Amino acid sequence alignment of BCM proteins in lettuce, Arabidopsis, soybean and tomato.

SupplementalFigure S12. Natural senescence of *lsbcm*, *lssgr*, and *lsbcm lssgr* mutants in lettuce.

SupplementalFigure S13. Characterization of *lsbcm* and *lssgr* mutants.

SupplementalTable S1. Primers used in genome editing and RT-qPCR.

Acknowledgments

We thank Yumi Nagashima for technical assistance, Kazuya Kiyokawa for helpful advice on the *Agrobacterium* strains, Benke Kuai (Fudan University) and Ayumi Tanaka (Hokkaido University) for providing the *nye1-1 nye2-1* double mutant, Yuichiro Takahashi (Okayama University) for providing the anti-PsaF antibody, and Masato Nakai (Osaka University) for providing the anti-TIC110 antibodies.

Funding

This research was supported by Research Fellowships from the Project of the Bio-oriented Technology Research Advancement Institution (Research Program on Development of Innovative Technology) awarded to M.K. and the Joint Research Program implemented by the Institute of Plant Science and Resources, Okayama University, awarded to M.K. and T.I.

Conflict of interest statement. None declared.

References

- Albrecht-Borth V, Kauss D, Fan D, Hu Y, Collinge D, Marri S, Liebers M, Apel K, Pfannschmidt T, Chow WS, et al.** (2013) A novel proteinase, SNOWY COTYLEDON4, is required for photosynthetic acclimation to higher light intensities in *Arabidopsis*. *Plant Physiol* **163**: 732–745
- Chen M, Choi YD, Voytas DF, Rodermel S** (2000) Mutations in the *Arabidopsis* VAR2 locus cause leaf variegation due to the loss of a chloroplast FtsH protease. *Plant J* **22**: 303–313
- Chen Y, Shimoda Y, Yokono M, Ito H, Tanaka A** (2019) Mg-dechelataase is involved in the formation of photosystem II but not in chlorophyll degradation in *Chlamydomonas reinhardtii*. *Plant J* **97**: 1022–1031
- Chen Y, Yamori W, Tanaka A, Tanaka R, Ito H** (2021) Degradation of the photosystem II core complex is independent of chlorophyll degradation mediated by Stay-Green Mg²⁺ dechelataase in *Arabidopsis*. *Plant Sci* **307**: 110902
- Chu CC, Li HM** (2011) Determining the location of an *Arabidopsis* chloroplast protein using in vitro import followed by fractionation and alkaline extraction. *Methods Mol Biol* **774**: 339–350
- Fukazawa J, Ohashi Y, Takahashi R, Nakai K, Takahashi Y** (2021) DELLA degradation by gibberellin promotes flowering via GAF1-TPR-dependent repression of floral repressors in *Arabidopsis*. *Plant Cell* **33**: 2258–2272
- Gao J, Wang H, Yuan Q, Feng Y** (2018) Structure and function of the photosystem supercomplexes. *Front Plant Sci* **9**: 357
- Horie Y, Ito H, Kusaba M, Tanaka R, Tanaka A** (2009) Participation of chlorophyll *b* reductase in the initial step of the degradation of light-harvesting chlorophyll *a/b*-protein complexes in *Arabidopsis*. *J Biol Chem* **284**: 17449–17456
- Jia T, Ito H, Tanaka A** (2016) Simultaneous regulation of antenna size and photosystem I/II stoichiometry in *Arabidopsis thaliana*. *Planta* **244**: 1041–1053
- Kato Y, Sun X, Zhang L, Sakamoto W** (2012) Cooperative D1 degradation in the photosystem II repair mediated by chloroplastic proteases in *Arabidopsis*. *Plant Physiol* **159**: 1428–1439
- Kikuchi S, Bédard J, Hirano M, Hirabayashi Y, Oishi M, Imai M, Takase M, Ide T, Nakai M** (2013) Uncovering the protein translocator at the chloroplast inner envelope membrane. *Science* **339**: 571–574
- Kohzuma K, Sato Y, Ito H, Okuzaki A, Watanabe M, Kobayashi H, Nakano M, Yamatani H, Masuda Y, Nagashima Y, et al.** (2017) The non-mendelian green cotyledon gene in soybean encodes a small subunit of photosystem II. *Plant Physiol* **173**: 2138–2147
- Kusaba M, Ito H, Morita R, Iida S, Sato Y, Fujimoto M, Kawasaki S, Tanaka R, Hirochika H, Nishimura M, et al.** (2007) Rice NON-YELLOW COLORING1 is involved in light-harvesting complex II and grana degradation during leaf senescence. *Plant Cell Online* **19**: 1362–1375
- Kusaba M, Tanaka A, Tanaka R** (2013) Stay-green plants: What do they tell us about the molecular mechanism of leaf senescence. *Photosynth Res* **117**: 221–234
- Liu G, Yu H, Yuan L, Li C, Ye J, Chen W, Wang Y, Ge P, Zhang J, Ye Z, et al.** (2021) *SIRCM1*, which encodes tomato Lutescent1, is required for chlorophyll synthesis and chloroplast development in fruits. *Hortic Res* **8**: 128
- Liu M, Wang Y, Nie Z, Gai J, Bhat JA, Kong J, Zhao T** (2020) Double mutation of two homologous genes *YL1* and *YL2* results in a leaf yellowing phenotype in soybean [*Glycine max* (L.) Merr]. *Plant Mol Biol* **103**: 527–543
- Majsec K, Bhuiyan NH, Sun Q, Kumari S, Kumar V, Ware D, van Wijk KJ** (2017) The plastid and mitochondrial peptidase network in *Arabidopsis thaliana*: a foundation for testing genetic interactions and functions in organellar proteostasis. *Plant Cell* **29**: 2687–2710
- Meguro M, Ito H, Takabayashi A, Tanaka R, Tanaka A** (2011) Identification of the 7-hydroxymethyl chlorophyll *a* reductase of the chlorophyll cycle in *Arabidopsis*. *Plant Cell* **23**: 3442–3453
- Morita R, Sato Y, Masuda Y, Nishimura M, Kusaba M** (2009) Defect in non-yellow coloring 3, an α/β hydrolase-fold family protein, causes a stay-green phenotype during leaf senescence in rice. *Plant J* **59**: 940–952
- Nakamura S, Mano S, Tanaka Y, Ohnishi M, Nakamori C, Araki M, Niwa T, Nishimura M, Kaminaka H, Nakagawa T, et al.** (2010) Gateway binary vectors with the bialaphos resistance gene, *bar*, as a selection marker for plant transformation. *Biosci Biotechnol Biochem* **74**: 1315–1319
- Nobusawa T, Kamei M, Ueda H, Matsushima N, Yamatani H, Kusaba M** (2021) Highly pleiotropic functions of CYP78As and AMP1 are regulated in non-cell-autonomous/organ-specific manners. *Plant Physiol* **186**: 767–781
- Olinares PDB, Ponnala L, Van Wijk KJ** (2010) Megadalton complexes in the chloroplast stroma of *Arabidopsis thaliana* characterized by size exclusion chromatography, mass spectrometry, and hierarchical clustering. *Mol Cell Proteomics* **9**: 1594–1615
- Ono K, Kimura M, Matsuura H, Tanaka A, Ito H** (2019) Jasmonate production through chlorophyll *a* degradation by Stay-Green in *Arabidopsis thaliana*. *J Plant Physiol* **238**: 53–62
- Osakabe Y, Watanabe T, Sugano SS, Ueta R, Ishihara R, Shinozaki K, Osakabe K** (2016) Optimization of CRISPR/Cas9 genome editing to modify abiotic stress responses in plants. *Sci Rep* **6**: 26685
- Park SY, Yu JW, Park JS, Li J, Yoo SC, Lee NY, Lee SK, Jeong SW, Seo HS, Koh HJ, et al.** (2007) The senescence-induced staygreen protein regulates chlorophyll degradation. *Plant Cell* **19**: 1649–1664
- Paulsen H, Finkenzeller B, Kühlein N** (1993) Pigments induce folding of light-harvesting chlorophyll *a/b*-binding protein. *Eur J Biochem* **215**: 809–816
- Ren G, An K, Liao Y, Zhou X, Cao Y, Zhao H, Ge X, Kuai B** (2007) Identification of a novel chloroplast protein AtNYE1 regulating chlorophyll degradation during leaf senescence in *Arabidopsis*. *Plant Physiol* **144**: 1429–1441
- Sakamoto W, Zaltsman A, Adam Z, Takahashi Y** (2003) Coordinated regulation and complex formation of YELLOW VARIEGATED1 and YELLOW VARIEGATED2, chloroplastic FtsH metalloproteases involved in the repair cycle of photosystem II in *Arabidopsis* thylakoid membranes. *Plant Cell* **15**: 2843–2855
- Saleh A, Alvarez-Venegas R, Avramova Z** (2008) An efficient chromatin immunoprecipitation (ChIP) protocol for studying histone modifications in *Arabidopsis* plants. *Nat Protoc* **3**: 1018–1025
- Sato Y, Morita R, Katsuma S, Nishimura M, Tanaka A, Kusaba M** (2009) Two short-chain dehydrogenase/reductases, NON-YELLOW COLORING 1 and NYC1-LIKE, are required for chlorophyll *b* and light-harvesting complex II degradation during senescence in rice. *Plant J* **57**: 120–131
- Sato Y, Morita R, Nishimura M, Yamaguchi H, Kusaba M** (2007) Mendel's green cotyledon gene encodes a positive regulator of the chlorophyll-degrading pathway. *Proc Natl Acad Sci USA* **104**: 14169–14174
- Schelbert S, Aubry S, Burla B, Agne B, Kessler F, Krupinska K, Hörtensteiner S** (2009) Pheophytin pheophorbide hydrolase (pheophytinase) is involved in chlorophyll breakdown during leaf senescence in *Arabidopsis*. *Plant Cell* **21**: 767–785
- Shimoda Y, Ito H, Tanaka A** (2016) *Arabidopsis* STAY-GREEN, Mendel's green cotyledon gene, encodes magnesium-dechelataase. *Plant Cell* **28**: 2147–2160
- Sun HJ, Cui ML, Ma B, Ezura H** (2006) Functional expression of the taste-modifying protein, miraculin, in transgenic lettuce. *FEBS Lett* **580**: 620–626
- Takechi K, Sodmergen, Murata M, Motoyoshi F, Sakamoto W** (2000) The YELLOW VARIEGATED (*VAR2*) locus encodes a homologue of FtsH, an ATP-dependent protease in *Arabidopsis*. *Plant Cell Physiol* **41**: 1334–1346
- Tanaka A, Yamamoto Y, Tsuji H** (1991) Formation of chlorophyll--protein complexes during greening. 2. Redistribution of chlorophyll among apoproteins. *Plant Cell Physiol* **32**: 195–204

- Tanaka R, Kobayashi K, Masuda T** (2011) Tetrapyrrole Metabolism in *Arabidopsis thaliana*. *Arab B* **9**: e0145
- Tsutsui H, Higashiyama T** (2016) pKAMA-ITACHI vectors for highly efficient CRISPR/Cas9-mediated gene knockout in *Arabidopsis thaliana*. *Plant Cell Physiol* pcw191
- Wang P, Grimm B** (2015) Organization of chlorophyll biosynthesis and insertion of chlorophyll into the chlorophyll-binding proteins in chloroplasts. *Photosynth Res* **126**: 189–202
- Wang M, Li W, Fang C, Xu F, Liu Y, Wang Z, Yang R, Zhang M, Liu S, Lu S, et al.** (2018) Parallel selection on a dormancy gene during domestication of crops from multiple families. *Nature Genet* **50**: 1435–1441
- Wang P, Richter AS, Kleeberg JRW, Geimer S, Grimm B** (2020) Post-translational coordination of chlorophyll biosynthesis and breakdown by BCMs maintains chlorophyll homeostasis during leaf development. *Nat Commun* **11**: 1254
- Waters MT, Langdale JA** (2009) The making of a chloroplast. *EMBO J* **28**: 2861–2873
- Waters MT, Wang P, Korkaric M, Capper RG, Saunders NJ, Langdale JA** (2009) GLK transcription factors coordinate expression of the photosynthetic apparatus in *Arabidopsis*. *Plant Cell* **21**: 1109–1128
- Wellburn AR** (1994) The spectral determination of chlorophylls *a* and *b*, as well as total carotenoids, using various solvents with spectrophotometers of different resolution. *J Plant Physiol* **144**: 307–313
- Wu S, Li Z, Yang L, Xie Z, Chen J, Zhang W, Liu T, Gao S, Gao J, Zhu Y, et al.** (2016) NON-YELLOWING2 (NYE2), a close paralog of NYE1, plays a positive role in chlorophyll degradation in *Arabidopsis*. *Mol Plant* **9**: 624–627
- Yamatani H, Kohzuma K, Nakano M, Takami T, Kato Y, Hayashi Y, Monden Y, Okumoto Y, Abe T, Kumamaru T, et al.** (2018) Impairment of Lhca4, a subunit of LHCl, causes high accumulation of chlorophyll and the stay-green phenotype in rice. *J Exp Bot* **69**: 1027–1035
- Yamatani H, Sato Y, Masuda Y, Kato Y, Morita R, Fukunaga K, Nagamura Y, Nishimura M, Sakamoto W, Tanaka A, et al.** (2013) NYC4, the rice ortholog of *Arabidopsis* THF1, is involved in the degradation of chlorophyll-Protein complexes during leaf senescence. *Plant J* **74**: 652–662
- Yoo SD, Cho YH, Sheen J** (2007) *Arabidopsis* mesophyll protoplasts: A versatile cell system for transient gene expression analysis. *Nat Protoc* **2**: 1565–1572
- Zhang C, Zhang B, Mu B, Zheng X, Zhao F, Lan W, Fu A, Luan S** (2020) A thylakoid membrane protein functions synergistically with GUN5 in chlorophyll biosynthesis. *Plant Commun* **1**: 100094